



## Article

# Fracture Evolution and Mechanical Properties of Mortar Containing Different Inclusions

Gang Yao <sup>1,2</sup>, Guifeng Wang <sup>1</sup>, Lihai Tan <sup>3,4</sup> , Yinfeng Zhang <sup>1</sup>, Ruizhi Wang <sup>1</sup> and Xiaohan Yang <sup>5,\*</sup> 

<sup>1</sup> School of Mines, China University of Mining and Technology, Xuzhou 221116, China; yaogang\_yk@163.com (G.Y.); wgfskl@cumt.edu.cn (G.W.); ts22020068a31@cumt.edu.cn (Y.Z.); ts23020053a31@cumt.edu.cn (R.W.)

<sup>2</sup> Zhaolou Coal Mine, Yanmei Heze Energy and Chemical Co., Ltd., Xuzhou 274700, China

<sup>3</sup> School of Civil, Mining and Environmental Engineering, University of Wollongong, Wollongong, NSW 2522, Australia; lt716@uowmail.edu.au

<sup>4</sup> School of Resource Environment and Safety Engineering, University of South China, Hengyang 412001, China

<sup>5</sup> School of Civil Engineering, The University of Queensland, Brisbane, QLD 4072, Australia

\* Correspondence: xiaohan.yang@uq.edu.au

**Abstract:** To study the influence of inclusions on the fracture evolution and mechanical properties of mortar structures, a series of uniaxial compression tests for mortar samples containing cylinder inclusions of varying mechanical properties were conducted. The digital image correlation (DIC) technique was employed for the analysis of deformation characteristics. In addition, failure modes for each sample were determined using self-documenting code. The result shows that inclusions filled in holes significantly influence the mechanical properties and failure characteristics of mortar structures as they can change the stress distribution and cracking process. Cracks are typically initiated at the boundaries of the inclusions but will only extend into the inclusion if it is less robust than the surrounding matrix. Sample strength increases significantly with an increase in sample strength when the inclusion's strength does not surpass that of the surrounding material. Once the inclusion's strength exceeds that of the surrounding matrix, the strength of the specimen remains relatively unchanged.

**Keywords:** mortar structures; inclusions; mechanical properties; crack process; failure pattern



**Citation:** Yao, G.; Wang, G.; Tan, L.; Zhang, Y.; Wang, R.; Yang, X. Fracture Evolution and Mechanical Properties of Mortar Containing Different Inclusions. *Appl. Sci.* **2024**, *14*, 3166. <https://doi.org/10.3390/app14083166>

Academic Editor: Dario De Domenico

Received: 23 February 2024

Revised: 28 March 2024

Accepted: 28 March 2024

Published: 9 April 2024



**Copyright:** © 2024 by the authors. Licensee MDPI, Basel, Switzerland. This article is an open access article distributed under the terms and conditions of the Creative Commons Attribution (CC BY) license (<https://creativecommons.org/licenses/by/4.0/>).

## 1. Introduction

Inclusions are commonly found in geo-materials such as rock and coal as well as artificial structures such as concrete buildings [1,2], tunneling [3,4], and mining roadways [5,6]. In underground environments, a dyke intrusion into sedimentary rock can create an inclusion that is denser and stronger than the surrounding material. Backfilling [7–9] and side-entry retaining [10–12] with the filling of engineering materials are widely used mining techniques that can generate an inclusion softer than the surrounding rock. In civil engineering, concrete structures generally contain different inclusions, such as aggregate [13,14], wood [1,15], and embedded materials [16].

The existence of inclusions will have a significant influence on the mechanical properties and failure characteristics of the whole natural or artificial structure, as inclusions can change the stress distribution and cracking process. Hence, it is highly worthwhile to study the influence of inclusions on the overall fracture evolution and mechanical properties. Few researchers have studied the influence of inclusions through experimental and numerical studies. Janeiro et al. [17] studied the influence of the shape and number of inclusions on the cracking behavior of prismatic gypsum subjected to a uniaxial compression load. Based on the experimental results conducted by Janeiro et al., Wu et al. [5] extended the numerical manifold method (NMM) to investigate the strength and cracking of samples containing either one or double cylinder inclusions under a uniaxial compression load. However, the

NMM model cannot obtain a satisfying prediction of the cracking behavior of samples containing stiff inclusions. Miao et al. [18] studied the effects of different filling materials (Gypsum, Cement, and Resin) on the mechanical properties and crack behavior of sandstone samples with a single filled flaw under a uniaxial compression load. Zhu et al. [19] performed uniaxial compression tests on sandstone samples containing single inclusions with various properties, including stiffness and shape. Most research has focused on the effect of the shape, number, and distribution of inclusions on crack mechanical properties and the cracking behavior of rock, concrete, mortar, or gypsum samples. More work needs to be conducted on the effect of inclusions with different strengths and elasticities on the crack evolution and mechanical properties of samples.

Digital image correlation (DIC) is a kind of non-contacting method that can achieve deformation measurements and stress intensity evaluations by performing a digital image analysis of observed objects [20]. DIC has been widely used to analyze the fracture and crack propagation of concrete [21,22] and rock [23] due to its advantages of non-contact, full-field measurement, simple devices, and strong anti-interference. Dario et al. [24] incorporated DIC techniques into three-point bending tests for notched concrete beams, which were reinforced with various strengthening systems, identifying failure at characteristic stress points. Similarly, Tan et al. [25,26] utilized DIC techniques to uncover the fracture behavior of rock samples containing cavities under both quasi-static and dynamic-loading conditions. These researches demonstrated that DIC can be successfully applied to analyze the fracture evolution of geo-materials and concrete.

In this study, mortar samples containing cylindrical inclusions of varying properties are tested under a uniaxial compression load to study the effect of inclusions on the fracture evolution and mechanical properties of samples using the DIC method. This research aims to understand the impact of inclusions on the mechanical characteristics and failure features of mortar. The presence and characteristics of inclusions are critical in many engineering applications, making this study significant for enhancing material designs and predicting structural performance.

## 2. Test Methodology

### 2.1. DIC Method

The DIC method, which is a fully non-destructive and non-contact measurement technique, can demonstrate the surface deformation of an object using a number of digital images from a reference undeformed and subsequent deformed states [23]. DIC can achieve a full field measurement [27]. DIC has been widely used to track the deformations of engineering materials, including rock, concrete, coal, and so on [28]. The more detailed fundamentals of DIC have been well-documented in the literature [29]. In the experimental study of this paper, the DIC method was applied to track the whole fracture process of mortar samples with different inclusions. A high-resolution Canon 60D camera, which can acquire digital images with  $1920 \times 1088$  pixels, was placed in front of the samples during the test to film the fracture initiation and propagation process on the sample's surface. The procedure of the DIC method is as follows:

1. Paint the surface of the sample with white paint.
2. Spray black dots on the white paint as reference points for the image analysis.
3. Place the camera and tripod in front of the sample. Additional light needs to be added to avoid shadow if necessary.
4. Film the sample surface during the loading process.
5. Visualize the fracture process on the sample surface using image correlation software.

In this study, the analysis of the recorded digital image data was conducted using the Ncorr v1.2.2 program [30]. This software, based on a parametric concept, can achieve a 2D evaluation of a digital image series of conventional cameras, high-speed cameras, or industrial image processing cameras. The DIC method adopted in this study is illustrated in Figure 1.

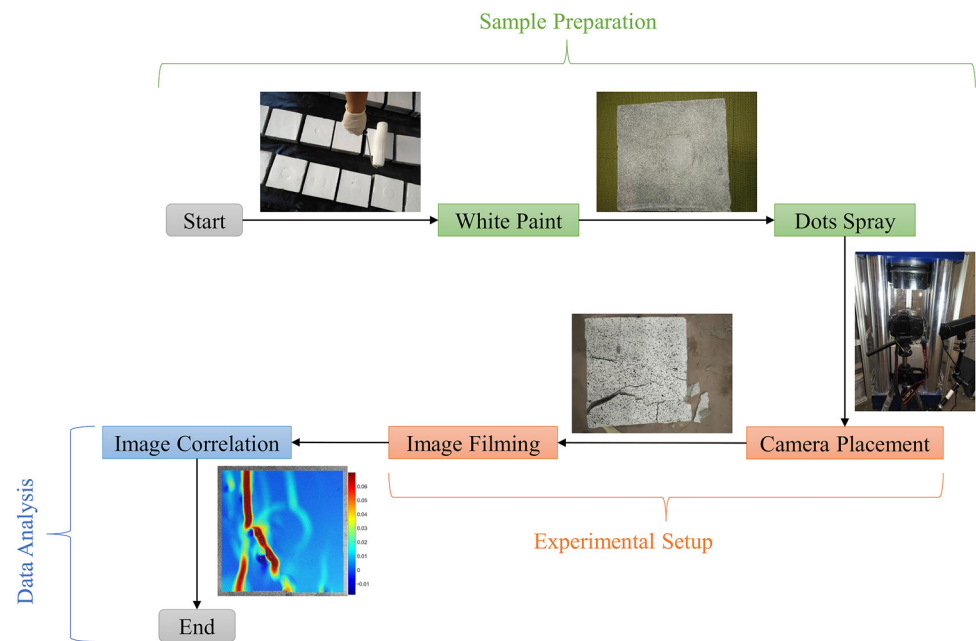


**Figure 1.** Flowchart of DIC method.

## 2.2. Sample Preparation

The samples containing different inclusions were prepared in a laboratory with Botany sand for rendering and concreting; general-purpose cement conforms to the AS 3972 standard [31] and water. The preparation of each sample includes two main steps: 1. The preparation of cylinder inclusions according to a designed mixing plan. 2. The casting of a mortar block containing an inclusion after the compaction of the inclusion. The sample preparation process is shown in Figure 2. The dimensions of the mortar samples are 100 mm (height)  $\times$  100 mm (width)  $\times$  30 mm (thickness). The size of the inclusion is 25 mm in diameter and 30 mm in height. The centroid of the inclusion is positioned in the centroid of the whole sample. The schematic diagram of the sample size and shape is shown in Figure 3.



**Figure 2.** Timber mold used to cast samples.

The inclusions are prepared according to the composition plan listed in Table 1. For each type of inclusion, two cylindrical samples (each 25 mm in diameter and 50 mm in

height) were prepared to ascertain their mechanical properties. The stress–strain curves of all inclusions are shown in Figure 4. The composition plan for the mortar blocks was identical to that of Group S3. Finally, as shown in Table 2, five group samples with different inclusions are prepared for the experimental study. Each group contains three samples. The sand was selected using sieves ranging from 50 to 100 mesh, resulting in a particle size of approximately between 0.15 and 0.30 mm.

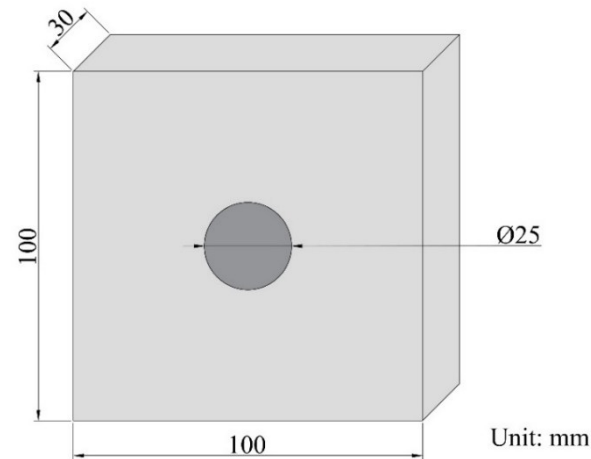


Figure 3. Geometry of a mortar sample containing an inclusion.

Table 1. Composition and mechanical properties of inclusions.

Inclusion Type	Cement/%	Sand/%	Water/%	Strength/MPa
I1	51.72	34.48	13.79	69.44
I2	41.67	41.67	16.66	53.97
I3	40.00	40.00	20.00	46.49
I4	38.46	38.46	23.08	40.11
I5	32.27	48.38	19.35	34.08

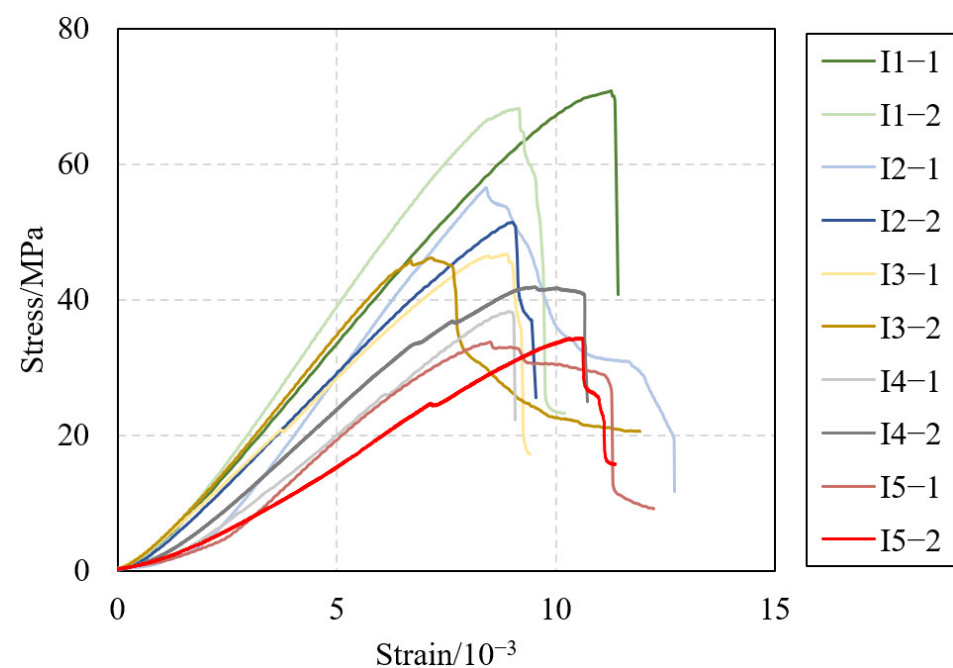


Figure 4. Stress–strain curves of all inclusions.

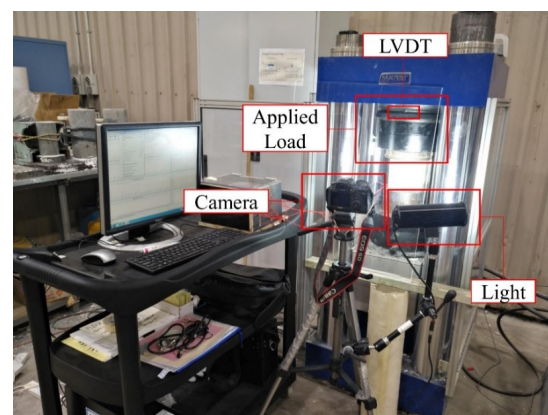


**Table 2.** Sample group with different inclusions.

Sample Group	S1	S2	S3	S4	S5
Inclusion Type	I1	I2	I3	I4	I5

### 2.3. Test Procedure

The experimental setup comprises two main components: the mechanic loading machine and the high-resolution camera, as depicted in Figure 5. The uniaxial compression tests were conducted by a MATEST C125N servo loading machine, which is manufactured by Matest, a company in Treviolo, Italy. Load–displacement data were obtained by the LVDT mounted on the upper loading plate. The loading rate is 0.1 mm/min with displacement control, ensuring that the specimen is subjected to quasi-static loading. The video is recorded by a high-resolution camera placed in front of the sample. These recordings are used to visually analyze the fracture process at the surface of the sample. To enhance the filming quality, additional light is used to improve the contrast between the samples and the background.

**Figure 5.** Experimental setup.

## 3. Test Results

### 3.1. Axial Stress–Strain Curves

The axial stress–strain curves of all samples containing different inclusions are shown in Figure 6. It can be seen from the stress–strain curves that the inclusion’s property has an obvious influence on the overall mechanical behavior of the intact samples. The average strengths of groups S1, S2, S3, S4, and S5 are 90, 85, 80, 58, and 41 MPa, respectively. The strength variation within each group does not exceed 4%, indicating that samples in the same group have similar mechanical properties. Group S1 samples contain the strongest inclusions and have the highest strength. Consequently, it can be concluded that the strength of samples containing inclusions increases with the mechanical properties of the inclusions, which is identical to the experimental studies in other studies [17].

The axial stress–strain curves of the samples can be divided into three stages, i.e., fissure closure, elastic deformation, and post-peak [19]. As shown in Figures 6 and 7, all the samples experienced these three stages during the loading process. In the fissure closure stage, the majority of existing defects in the mortar samples are compressed by applied stress with a low level. Hence, the stress–strain curves at this stage are in a non-linear relationship. Then, the stress–strain curves turn into the elastic deformation stage. In this stage, the deformation of the mortar samples grows almost linearly with the increase in the applied uniaxial load until it reaches the peak. It can be seen from Figure 7 that the pre-peak elasticity of the samples is also influenced by the properties of the inclusions. The consistency of the stress–strain curves within groups S1, S2, and S3 is better than groups S4 and S5, which might be caused by the dominant effect of strong inclusions. Moreover, the

stress–strain curves of groups S1 and S2 only have one sudden drop during the post-peak stage, whereas the curves for the other groups tend to show a more gradual decline, often in two or more stages.

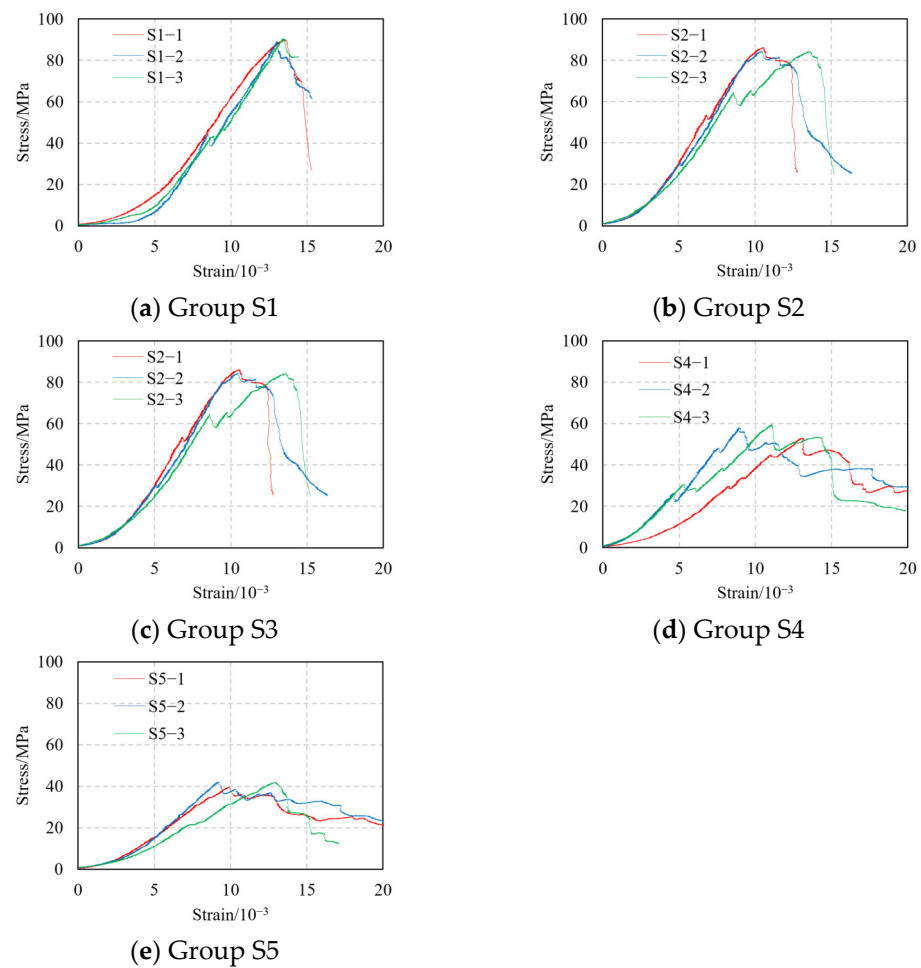


**Figure 6.** Stress–strain curves of samples with different inclusions.

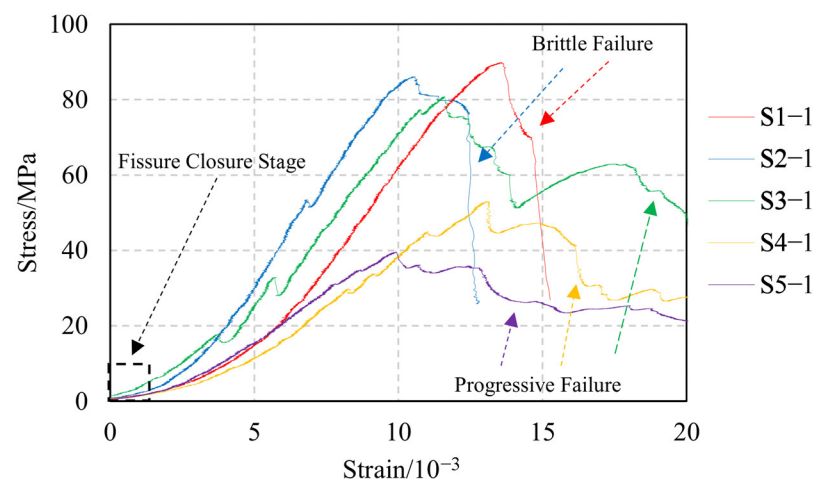
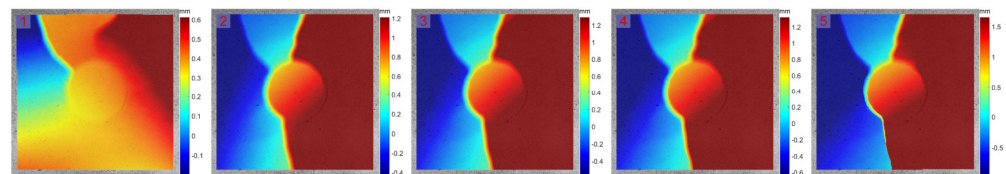


**Figure 7.** Stress–strain curves of mortar samples.

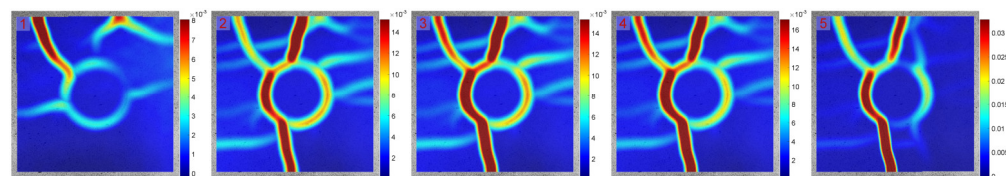
### 3.2. Cracking Process

In this study, the cracking process around the different inclusions is analyzed with the DIC method, as the development of micro cracks is hardly visible to the naked eye. The

processed images of samples S1-1, S3-1, and S5-1 are shown in Figures 8–10, respectively. For each sample, the displacement and strain contours at five evenly selected loading time points from the onset of a localized strain concentration to the end of the test are presented to illustrate the deformation and failure evolution process throughout the entire test. By combining the displacement contours in the X direction with the strain contours, it is evident that the main cracking path in all three samples is almost parallel to the loading direction. Under uniaxial compression, the macroscopic failure of all samples is predominantly characterized by splitting tensile failure.

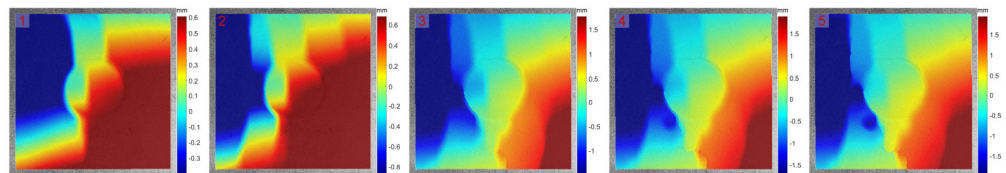


(a) Displacement contours in X direction

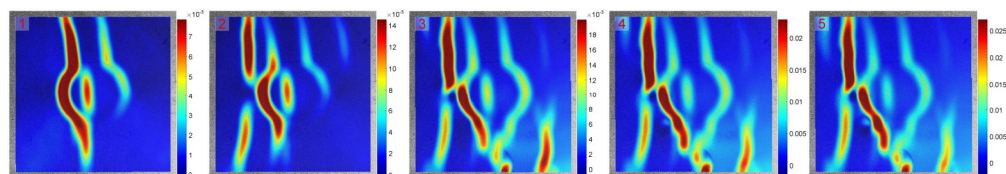


(b) Maximum principal strain contours

**Figure 8.** Fracture process of sample S1-1.



(a) Displacement contours in X direction



(b) Maximum principal strain contours

**Figure 9.** Fracture process of sample S3-1.

The comparison among samples containing various inclusions reveals that the strength of the inclusions notably influences the initiation and progression of the cracks. For sample S1-1, the tensile cracks propagate parallel to the loading direction but are confined to the mortar matrix, never crossing the inclusion boundary. Conversely, for samples S3-1 and S5-1, the tensile cracks extend parallel to the loading direction, affecting both the inclusions and the surrounding mortar. Specifically, for sample S5-1, the crack is initiated from the inclusion or inclusion boundary to the mortar sample.

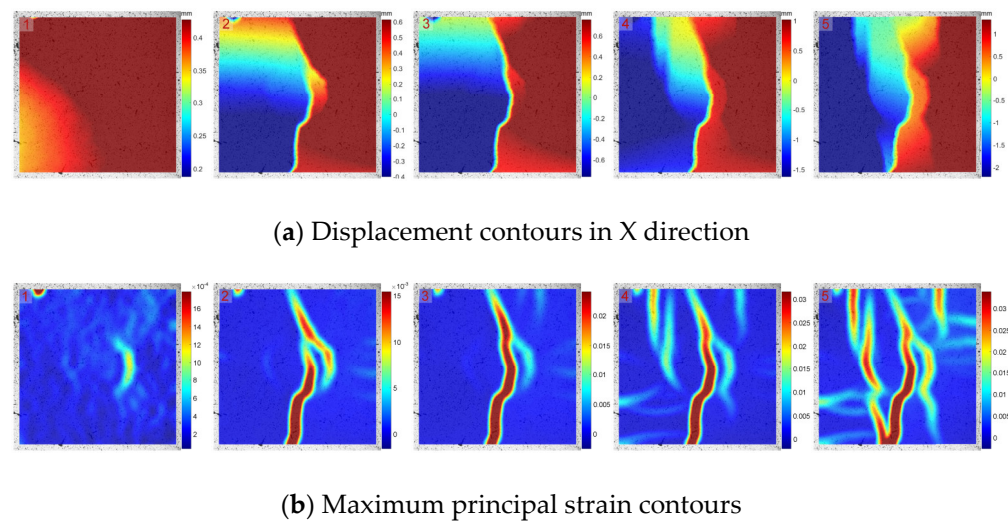


**Figure 10.** Fracture process of sample S5-1.

In addition, it has been mentioned in the literature that the mechanical properties of rock with an opening are closely related to the stress distribution around the opening [32]. For the weaker inclusion, the tensile cracks would initiate at the top or bottom of the interface as high tangential tensile stress occurs and is concentrated in these areas [17]. This pattern is observed in samples S3-1 and S5-1, where the tensile crack, indeed, initiates at the top and bottom locations surrounding the weaker cylindrical inclusions. However, for sample S2-1, the cracks are initiated from the inclusion boundary. Additionally, it is evident from these figures that the number of cracks in the samples significantly increases during the loading process, and the crack distribution pattern of samples with stronger inclusions is more complicated than that of weaker inclusions. This is primarily because samples containing stronger inclusions are capable of withstanding greater loads without the formation of cracks.

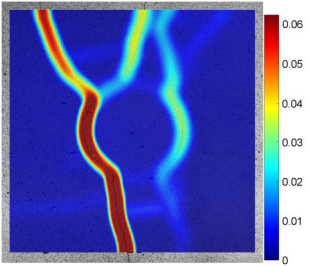
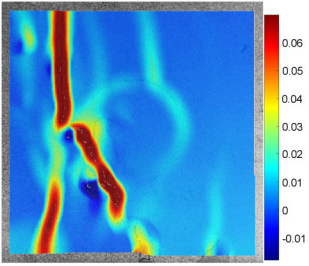
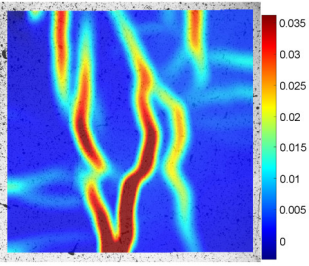
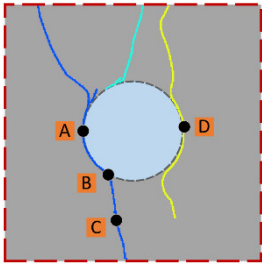
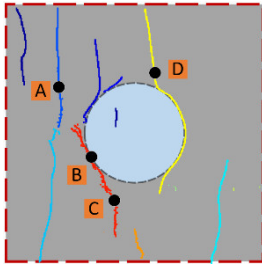
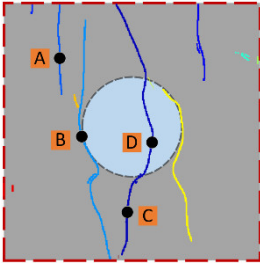
### 3.3. Failure Pattern

The final failure patterns of samples containing different inclusions are presented in Table 3. Points A–D on each sample are measurement circles positioned on the paths of cracks. To avoid the potential error of the manual selection of fractures, the failure patterns are automatically recognized by self-documenting code based on MATLAB 2018b. In the failure pattern, the independent fractures in each sample are distinguished by different colors.

It can be seen from Table 3 that the failure pattern of the samples is very similar to the corresponding DIC analysis of the strain contour. For sample S1-1, the final failure of the sample is caused by three major tensile cracks. The cracks on the left form an approximate “Y” shape along the inclusion’s left boundary, and another crack is basically along the tangent of the boundary on the right side of the boundary. The inclusions are not penetrated through by these macro cracks due to the support of the inclusion with higher strength. For sample S3-1, the final failure of the sample is caused by an inverted “Y” shape crack on the left side of the sample. The inverted “Y” shape crack is initiated and propagated parallel to the loading direction at the beginning but deflects towards the inclusion when approaching the loading ends of the sample. An independent crack is observed in the inclusion but fails to reach the boundary. In sample S4-1, the crack’s distribution is more complicated than in the other sample. Several cracks rapidly propagate along the loading direction and penetrate through the entire sample, including the inclusion.



Table 3. Failure pattern of samples with different inclusions.

Sample	S1-1	S3-1	S5-1
DIC Analysis			
Failure pattern			

While current DIC technology can effectively capture the deformation process on the surface of samples, a deeper investigation into the initiation and progression of cracks within damaged areas is necessary. To address this, a measurement circle method was proposed to reveal the strain characteristics of cracks for a better understanding of the fracturing process in this study. As shown in Figure 11, a measurement circle is a small circular set on the crack path in the ROI area of the sample surface, and the average strain calculated by the subsets (a set of pixels) inside the measurement circle is the strain value of the measurement circle area. The evolution of the cracks is further studied by monitoring the changes in the strain value inside the measurement circle. Figure 12 shows the evolution of the internal strain curve of the measurement circle with different radii at the same monitoring point. Despite a similar developing trend, the curves from the circles of different radii exhibit a significant difference in terms of value. Since the strain value indicates the average strain within the measurement circle, the curves for measurement circles with a larger radius tend to flatten, which may be insufficient in describing the characteristics of the deformation evolution of the crack. Taking this influence into consideration, the measurement circle with a 1.0 mm radius is selected. As shown in Table 3, in this study, four typical measurement circles (A, B, C, and D) are installed for the cracks of each sample to further explore the evolution of the failure pattern.

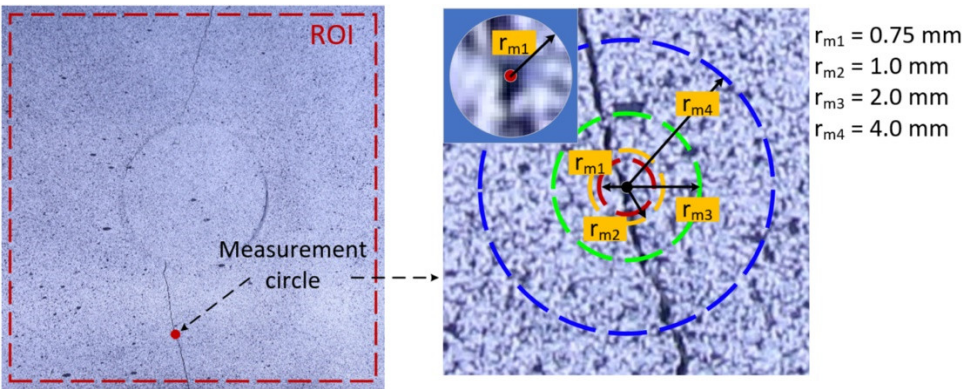
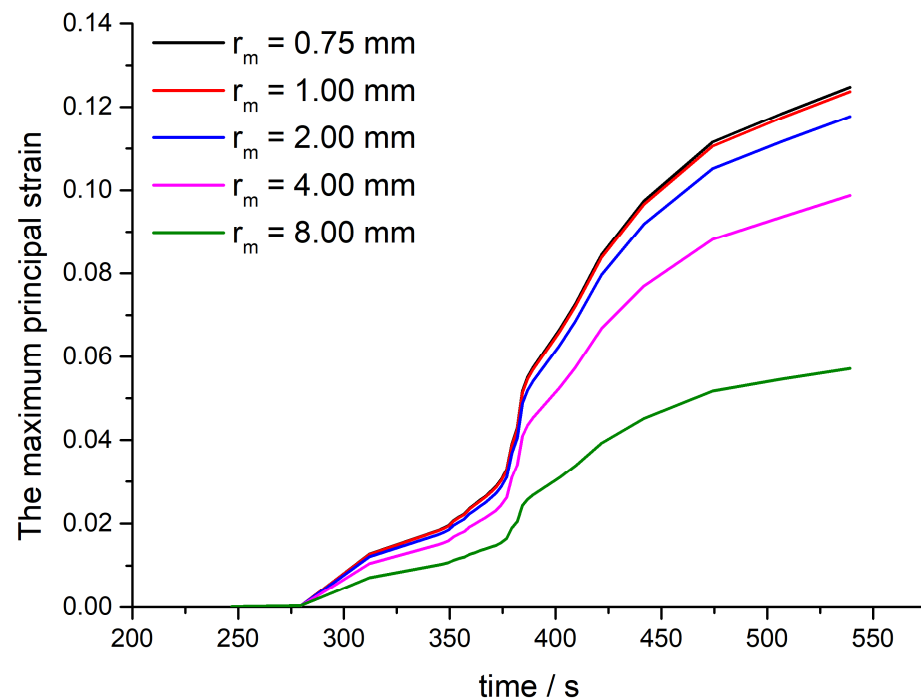


Figure 11. Schematic diagram of measurement circles on a crack path.



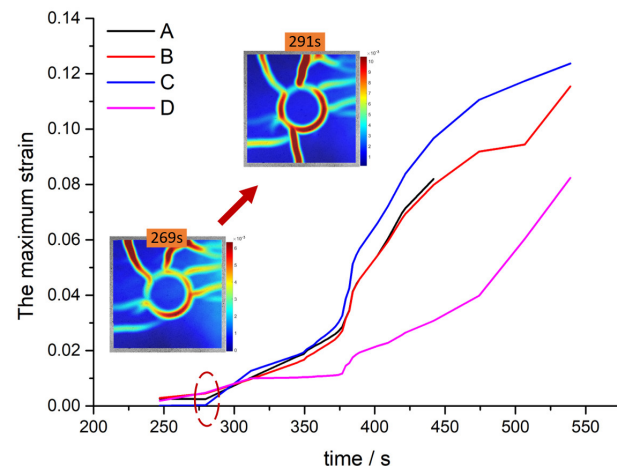


**Figure 12.** Strain evolution curves of measurement circles with different radii at the same location.

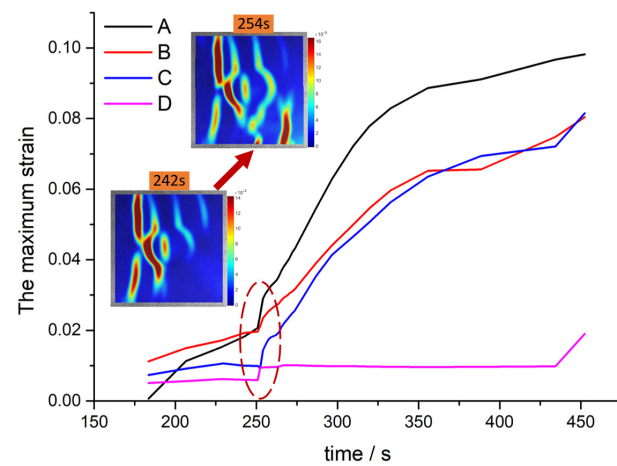
Figure 13 shows the curves of the maximum principal strain over time for these measurement circles as well as the sudden change in the maximum principal strain contours during key stages. A notable observation is that a turning point on the strain curve typically signals the abrupt emergence of a concentrated strain area. For example, for sample S1-1, as the loading time reaches approximately 270 s, the strain curves on all four measurement circles begin to show a marked increase from a stable state. Comparing the strain contour maps between 269 s and 291 s, it becomes evident that a high-strain concentration zone suddenly emerges beneath the inclusion at this time, suggesting the potential formation of a crack in this area. Similar phenomena have been observed in other samples as well.

Observing the strain curves of the four measurement circles for each of the three samples in Figure 13 reveals a trend in some of the circles that can be characterized as a sequence of calm to rapid rise to slow rise to rapid rise. This pattern is evident in measurement circles B and D of sample S1-1, B and C of sample S3-1, and B and D of sample S5-1. This trend reflects the complete process of a crack evolution: the initial rapid increase from a calm state indicates the onset of a strain concentration in the area of the measurement circle. This is followed by a relatively slow and stable increase, suggesting that the concentrated strain area is gradually forming a crack and extending stably. The subsequent rapid increase indicates that the crack in the sample has entered a late, unstable expansion phase in that region, and the material in the area has lost its load-bearing capacity. Overall, these curves comprehensively depict the complete process of a crack evolution, from initial appearance through stable development to unstable progression.

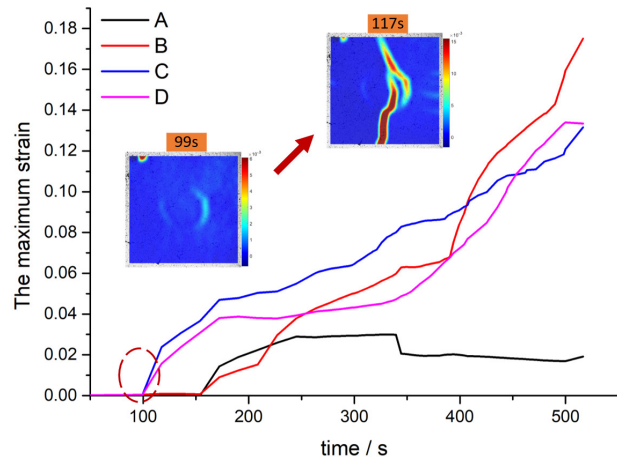
It should be noted that not all measurement circles' strain curves exhibit this complete trend. For some circles, such as measurement circle C in sample S1-1, circle A in S3-1, and circle C in S5-1, the strain curves do not clearly show the unstable phase of crack development by the end of the tests, which is when the samples as a whole have already been broken. This could be due to the emergence of major macroscopic cracks in other regions of the sample. When such major cracks appear, the failure of the sample tends to concentrate around these cracks, ultimately leading to the overall instability of the sample. As a result, the development of cracks in other regions may be suppressed to a certain extent, preventing them from progressing to an unstable phase and forming major macroscopic failure cracks.



(a) S1-1



(b) S3-1



(c) S5-1

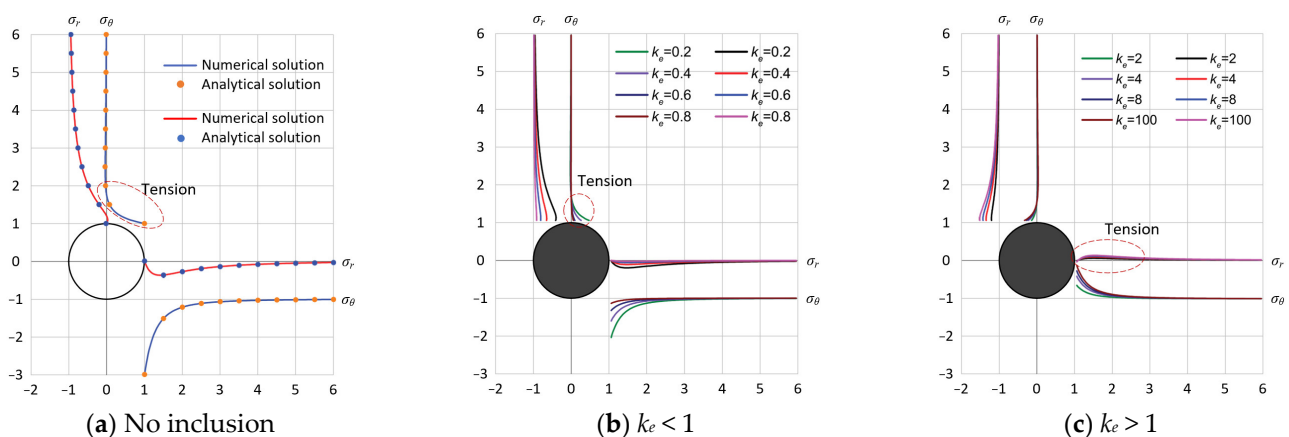
**Figure 13.** Maximum principal strain vs. time curves of samples.

#### 4. Discussion

The influence of the inclusion on the strength of the sample mainly depends on its influence on the stress distribution around the hole. The stress solution in the area around the rigid inclusion ( $E = \infty$ ) in an infinite field has been provided in the literature [17], which indicated that a rigid backfilled inclusion changes the stress concentration around

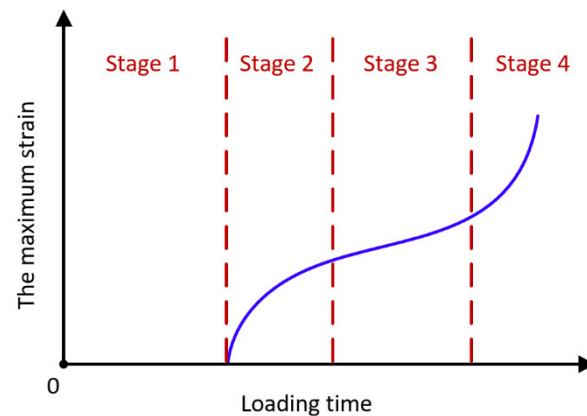
the inclusion and thus changes the rock's stability and failure behavior. However, in practical engineering, the inclusion cannot be regarded as rigid material in most cases, where deformation modules of the inclusion are various and may have different influences on the surrounding materials from case to case. To further determine the influence of inclusion elasticity on the stress distribution around the inclusion, the stress distribution characteristics around the hole-containing incursion with varying elastic moduli are discussed.

Figure 14 demonstrates the stress curves of the top and side corners of a unit circular hole in an infinite plate subject to a vertical far field uniaxial, compressive stress  $\sigma_0$  with different  $k_e$  ( $k_e$  refers to the ratio of the elastic modulus of the inclusion to that of the external material). Figure 14a presents the stress curves for both numerical and analytical solutions in the absence of an inclusion. The numerical solution is obtained through finite element numerical methods, while the analytical solution is derived using complex variable function methods [33,34]. Figure 14b,c depicts scenarios where the elastic modulus of the inclusion is less than ( $k_e < 1$ ) and greater than ( $k_e > 1$ ) the elastic modulus of the external material, respectively.  $\sigma_\theta$  and  $\sigma_r$  refer to the hoop stress and radial stress within the plane, respectively. It can be seen from Figure 14a that for the plate containing a single circular hole, a strong compressive stress concentration can be observed in the middle point of the hole sides ( $\sigma_\theta = 3\sigma_0$ ), while tensile stress concentration was formed in the top and bottom of the hole ( $\sigma_\theta = -\sigma_0$ ). Hence, the bottom and top corners experienced a tensile crack, while the side corners of the opening experienced splitting damage due to the compression stress concentration [35–37]. However, the existence of the inclusion will change the stress distribution around the inclusion and thus change its failure behavior. As shown in Figure 14b, when  $k_e$  was less than 1.0, the stress concentration in both the side and top points decreased with the increase in  $k_e$ , indicating the support from the inclusion is improving. When  $k_e$  was greater than 1.0 (Figure 14c),  $\sigma_\theta$  in the top point was transferred to compressive stress and increased slightly with the increase in  $k_e$ . Meanwhile, as for the middle point in the side,  $\sigma_\theta$  in the form of compressive stress decreased, but  $\sigma_r$  tended to have tensile stress under a low level near the middle side point along the horizontal line. Compared with Figure 8, it can be seen that for the samples with a strong inclusion, an initial strain concentration appeared around the inclusion sides but failed to form macro-cracks.



**Figure 14.** Stress distribution around an opening or inclusion.

According to the maximum principal strain versus time curves and maximum principal strain contours, the crack propagation process can be divided into four stages with an increase in the loading time as shown in Figure 15.



**Figure 15.** Evolution characteristics of the maximum principal strain at monitoring points on a crack path.

Stage 1—Quiet stage: Strain concentration has not yet appeared, and the principal strain remains at a very low level.

Stage 2—Formation Stage of the Stress Concentration Area: The principal strain suddenly increases. Strain concentration begins to manifest at the location predisposed to a crack formation.

Stage 3—Stable Propagation Stage of Cracks: The strain curve during this phase exhibits an approximately linear rise, which is indicative of the crack progressing in a steady and controlled manner. This stage reflects the period during which the material undergoes predictable and manageable crack growth.

Stage 4—Rapid Propagation Stage of Cracks: The slope of the curve suddenly increases. The visible cracks appear as the width of the cracks increases rapidly. The entire sample has entered an irreversible instability state. This stage is not necessary as failure may be non-violent on the crack path, or the test may be stopped before this stage.

Overall, it has been observed that inclusions significantly influence the mechanical behavior of mortar structures. When there is a substantial difference between the mechanical properties of the inclusions and the surrounding material, the strain distribution characteristics and the paths of crack development are notably altered. The overall evolution of cracks follows a discernible pattern, and the stages of crack propagation identified in this study are seen to provide essential insights into the predictive maintenance of mortar structures. Through the recognition of early indicators of deformation concentration and crack initiation, timely interventions can be implemented to avert catastrophic failures. Moreover, the incorporation of reinforcing materials, such as steel fibers into concrete, is known to significantly enhance mechanical properties [38], introducing a layer of complexity to the interactions between the surrounding matrix and inclusions as well as the overall mechanical behavior of the structure, which merits further exploration. An in-depth comprehension of such a material's mechanical behavior when containing inclusions is found to contribute to the enhancement of durability and safety in mortar infrastructures, thereby prolonging their operational life and minimizing long-term maintenance expenditures.

## 5. Conclusions

In this study, mortar samples with different cylindrical inclusions were tested under a uniaxial compression load to study the effect of inclusions on fracture evolution and mechanical properties of mortar structures with the application of the DIC method. The measurement circle method was proposed to further explore the evolution of fractures. The following conclusions can be drawn based on this paper:

1. The existence of inclusions can significantly improve the stress concentration around the opening and increase the strength of the mortar sample. However, this improve-

ment in overall strength is not very obvious when the inclusion is stronger than the external material.

2. The inclusion has a significant influence on the fracture pattern of the sample. When the inclusion is weaker than the external material, the inside of the inclusion will undergo penetrated tensile failure along the loading direction. The failure mode of the external part is similar to the samples without an inclusion. The top and the bottom of the opening are characterized by tensile failure, but the splitting failure around the left boundary of the opening is not apparent due to the restraint effect of the inclusion. The debonding failure along the interface is not conspicuous either. When the mechanical properties of the inclusion are consistent with the external material, the debonding failure can be found. Under the influence of the interface, the presence of failure within the inclusion is unlikely to lead to contiguous deformation or a pronounced failure that extends through to the external material.
3. The results of the strain evolution of the measurement circle along the fracture path show that, under uniaxial static compression, the fracture's propagation can be divided into four stages: the quiet stage, the formation stage of the stress concentration area, the stable crack propagation stage, and the rapid crack propagation stage.
4. The strength of the intact sample is higher than that of all samples containing inclusions, even if the inclusions are identical or stronger than the external material. This shows that the discontinuity of the mechanical properties of the inclusions and the external material may have a certain weakening effect on the overall mechanical properties of the sample, which suggests more attention should be given to the coordinated force and deformation between the backfilling material and the surrounding rock in related projects.
5. By strategically arranging measurement circles along the crack path and employing DIC technology, the deformation characteristics within the fracture zone can be accurately captured, allowing for effective monitoring of the crack's entire evolution process. In future studies, this approach can be further optimized by incorporating displacement vector fields around the cracks, enabling the classification of crack types to be determined.

**Author Contributions:** Conceptualization, G.Y.; Methodology, G.Y., L.T. and X.Y.; Software, Y.Z.; Validation, Y.Z.; Formal analysis, R.W.; Data curation, L.T. and R.W.; Writing—original draft, L.T. and X.Y.; Writing—review & editing, G.W. and Y.Z.; Supervision, G.W. All authors have read and agreed to the published version of the manuscript.

**Funding:** This research was funded by Hunan provincial department of education, grant number 23B0442.

**Institutional Review Board Statement:** Not applicable.

**Informed Consent Statement:** Not applicable.

**Data Availability Statement:** The data presented in this study are available in the article.

**Conflicts of Interest:** Author Yao Gang was employed by the company Zhaolou Coal Mine, Yanmei Heze Energy and Chemical Co., Ltd. The remaining authors declare that the research was conducted in the absence of any commercial or financial relationships that could be construed as a potential conflict of interest.

## References

1. Erlbeck, L.; Schreiner, P.; Schlachter, K.; Dörnhöfer, P.; Fasel, F.; Methner, F.J.; Rädle, M. Adjustment of thermal behavior by changing the shape of PCM inclusions in concrete blocks. *Energy Convers. Manag.* **2018**, *158*, 256–265. [\[CrossRef\]](#)
2. Chen, L.; Su, R.K.L. Service life modelling of carbonated reinforced concrete with supplementary cementitious materials considering early corrosion propagation. *Constr. Build. Mater.* **2024**, *413*, 134861. [\[CrossRef\]](#)
3. Xu, M.; Liu, X.S. Experimental and Theoretical Solutions on Collapse Mechanism of Tunnelling with Embedded Forepoles. *J. Civ. Archit. Environ. Eng.* **2013**, *35*, 25–31. [\[CrossRef\]](#)
4. Beer, G.; Marussig, B.; Zechner, J.; Dünser, C.; Fries, T.P. Isogeometric boundary element analysis with elasto-plastic inclusions. Part 1: Plane problems. *Comput. Methods Appl. Mech. Eng.* **2016**, *308*, 552–570. [\[CrossRef\]](#)



5. Wu, Z.J.; Wong, L.N.Y. Modeling cracking behavior of rock mass containing inclusions using the enriched numerical manifold method. *Eng. Geol.* **2013**, *162*, 1–13. [\[CrossRef\]](#)
6. Li, Z.; Ren, T.; Li, X.; Cheng, Y.; He, X.; Lin, J.; Qiao, M.; Yang, X. Full-scale pore structure characterization of different rank coals and its impact on gas adsorption capacity: A theoretical model and experimental study. *Energy* **2023**, *277*, 127621. [\[CrossRef\]](#)
7. Ju, F.; Huang, P.; Guo, S.; Xiao, M.; Lan, L.X. A roof model and its application in solid backfilling mining. *Int. J. Min. Sci. Technol.* **2017**, *27*, 139–143. [\[CrossRef\]](#)
8. Li, L. Generalized solution for mining backfill design. *Int. J. Geomech.* **2014**, *14*, 04014006. [\[CrossRef\]](#)
9. Zhu, X.J.; Guo, G.L.; Liu, H.; Yang, X.Y. Surface subsidence prediction method of backfill-strip mining in coal mining. *Bull. Eng. Geol. Environ.* **2019**, *78*, 6235–6248. [\[CrossRef\]](#)
10. Wang, Q.; He, M.C.; Yang, J.; Gao, H.K.; Jiang, B.; Yu, H.C. Study of a no-pillar mining technique with automatically formed gob-side entry retaining for longwall mining in coal mines. *Int. J. Rock Mech. Min. Sci.* **2018**, *110*, 1–8. [\[CrossRef\]](#)
11. Zhang, N.; Yuan, L.; Han, C.L.; Xue, J.H.; Kan, J.G. Stability and deformation of surrounding rock in pillarless gob-side entry retaining. *Saf. Sci.* **2012**, *50*, 593–599. [\[CrossRef\]](#)
12. Yang, H.Y.; Cao, S.G.; Wang, S.Q.; Fan, Y.C.; Wang, S.; Chen, X.Z. Adaptation assessment of gob-side entry retaining based on geological factors. *Eng. Geol.* **2016**, *209*, 143–151. [\[CrossRef\]](#)
13. Kan, Y.C.; Pei, K.C.; Chang, C.L. Strength and fracture toughness of heavy concrete with various iron aggregate inclusions. *Nucl. Eng. Des.* **2004**, *228*, 119–127. [\[CrossRef\]](#)
14. Xiao, J.Z.; Li, W.G.; Corr, D.J.; Shah, S.P. Effects of interfacial transition zones on the stress–strain behavior of modeled recycled aggregate concrete. *Cem. Concr. Res.* **2013**, *52*, 82–99. [\[CrossRef\]](#)
15. Lagier, F.; Massicotte, B.; Charron, J.P. Experimental investigation of bond stress distribution and bond strength in unconfined UHPFRC lap splices under direct tension. *Cem. Concr. Compos.* **2016**, *74*, 26–38. [\[CrossRef\]](#)
16. Raphael, F.L.; Luca, S.; David, C. Development of electrically conductive concrete and mortars with hybrid conductive inclusions. *Constr. Build. Mater.* **2020**, *237*, 117470.
17. Janeiro, R.P.; Einstein, H.H. Experimental study of the cracking behavior of specimens containing inclusions (under uniaxial compression). *Int. J. Fract.* **2010**, *164*, 83–102. [\[CrossRef\]](#)
18. Miao, S.T.; Pan, P.Z.; Wu, Z.H.; Li, S.J.; Zhao, S.K. Fracture analysis of sandstone with a single filled flaw under uniaxial compression. *Eng. Fract. Mech.* **2018**, *204*, 319–343. [\[CrossRef\]](#)
19. Zhu, Q.Q.; Li, D.Y.; Han, Z.Y.; Li, X.B.; Zhou, Z.L. Mechanical properties and fracture evolution of sandstone specimens containing different inclusions under uniaxial compression. *Int. J. Rock Mech. Min. Sci.* **2019**, *115*, 33–47. [\[CrossRef\]](#)
20. Wada, H.; Matsumoto, T.; Yamashita, Y. Diagnosis and treatment of disseminated intravascular coagulation (DIC) according to four DIC guidelines. *J. Intensive Care* **2014**, *2*, 15. [\[CrossRef\]](#)
21. Li, D.Y.; Huang, P.Y.; Chen, Z.B.; Yao, G.W.; Guo, X.Y.; Zheng, X.H.; Yang, Y. Experimental study on fracture and fatigue crack propagation processes in concrete based on DIC technology. *Eng. Fract. Mech.* **2020**, *235*, 107166. [\[CrossRef\]](#)
22. Skarżyński, Ł.; Tejchman, J. Experimental Investigations of Fracture Process Using DIC in Plain and Reinforced Concrete Beams under Bending. *Strain* **2013**, *49*, 521–543. [\[CrossRef\]](#)
23. Munoz, H.; Taheri, A.; Chanda, E.K. Pre-peak and post-peak rock strain characteristics during uniaxial compression by 3D digital image correlation. *Rock Mech. Rock Eng.* **2016**, *49*, 2541–2554. [\[CrossRef\]](#)
24. De Domenico, D.; Urso, S.; Borsellino, C.; Spinella, N.; Recupero, A. Bond behavior and ultimate capacity of notched concrete beams with externally-bonded FRP and PBO-FRCM systems under different environmental conditions. *Constr. Build. Mater.* **2020**, *265*, 121208. [\[CrossRef\]](#)
25. Tan, L.; Zhou, Z.; Cai, X.; Rui, Y. Analysis of mechanical behaviour and fracture interaction of multi-hole rock mass with DIC measurement. *Measurement* **2022**, *191*, 110794. [\[CrossRef\]](#)
26. Tan, L.; Ren, T.; Dou, L.; Cai, X.; Yang, X.; Zhou, Q. Dynamic response and fracture evolution of marble specimens containing rectangular cavities subjected to dynamic loading. *Bull. Eng. Geol. Environ.* **2021**, *80*, 7701–7716. [\[CrossRef\]](#)
27. Destrebecq, J.F.; Toussaint, E.; Ferrier, E. Analysis of cracks and deformations in a full scale reinforced concrete beam using a digital image correlation technique. *Exp. Mech.* **2011**, *51*, 879–890. [\[CrossRef\]](#)
28. David, C.; Matteo, A.; Lori, G.-B.; Surendra, S. Digital image correlation analysis of interfacial debonding properties and fracture behavior in concrete. *Eng. Fract. Mech.* **2007**, *74*, 109–121.
29. Schreier, H.; Orteu, J.J.; Sutton, M.A. *Image Correlation for Shape, Motion and Deformation Measurements: Basic Concepts, Theory and Applications*; Springer: Berlin/Heidelberg, Germany, 2009; Volume 1.
30. Blaber, J.; Adair, B.; Antoniou, A. Ncorr: Open-Source 2D Digital Image Correlation Matlab Software. *Exp. Mech.* **2015**, *55*, 1105–1122. [\[CrossRef\]](#)
31. AS 3972-2010; General Purpose and Blended Cements. Standards Australia: Sydney, Australia, 2010.
32. Zhu, W.C.; Liu, J.S.; Tang, C.A.; Zhao, X.D.; Brady, B.H. Simulation of progressive fracturing processes around underground excavations under biaxial compression. *Tunn. Undergr. Space Technol.* **2005**, *20*, 231–247. [\[CrossRef\]](#)
33. Tan, L.; Ren, T.; Dou, L.; Yang, X.; Qiao, M.; Peng, H. Analytical stress solution and mechanical properties for rock mass containing a hole with complex shape. *Theor. Appl. Fract. Mech.* **2021**, *114*, 103002. [\[CrossRef\]](#)
34. Tan, L.; Ren, T.; Dou, L.; Yang, X.; Wang, G.; Peng, H. Analytical Stress Solution and Numerical Mechanical Behavior of Rock Mass Containing an Opening under Different Confining Stress Conditions. *Mathematics* **2021**, *9*, 2462. [\[CrossRef\]](#)

35. Carter, B.J.; Lajtai, E.Z.; Yuan, Y. Tensile fracture from circular cavities loaded in compression. *Int. J. Fract.* **1992**, *57*, 221–236. [[CrossRef](#)]
36. Dzik, E.; Lajtai, E. Primary fracture propagation from circular cavities loaded in compression. *Int. J. Fract.* **1996**, *79*, 49–64. [[CrossRef](#)]
37. Lotidis, M.A.; Nomikos, P.P.; Sofianos, A.I. Numerical Simulation of Granite Plates Containing a Cylindrical Opening in Compression. *Procedia Eng.* **2017**, *191*, 242–247. [[CrossRef](#)]
38. Chen, G.; Gao, D.; Zhu, H.; Song Yuan, J.; Xiao, X.; Wang, W. Effects of novel multiple hooked-end steel fibres on flexural tensile behaviour of notched concrete beams with various strength grades. *Structures* **2021**, *33*, 3644–3654. [[CrossRef](#)]

**Disclaimer/Publisher’s Note:** The statements, opinions and data contained in all publications are solely those of the individual author(s) and contributor(s) and not of MDPI and/or the editor(s). MDPI and/or the editor(s) disclaim responsibility for any injury to people or property resulting from any ideas, methods, instructions or products referred to in the content.